ADVANCED ELECTRONIC MATERIALS
Open Access
www.advelectronicmat.de

Check for updates

Scalable Metal–Organic Chemical Vapor Deposition of High Quality $PtSe_2$

*Maximilian Prechtl, Stefan Heiserer, Marc Busch, Oliver Hartwig, Cormac Ó Coileáin, Tanja Stimpel-Lindner, Kuanysh Zhussupbekov, Kangho Lee, Ainur Zhussupbekova, Samuel Berman, Igor V. Shvets, and Georg S. Duesberg**

Platinum diselenide ($PtSe_2$), a 2D noble metal dichalcogenide, has recently received significant attention due to its outstanding properties. It undergoes a semimetal to semiconductor transition when thinned, offers a bandgap in the infrared range, and exhibits excellent stability in ambient conditions. These properties make it a prime active material in optoelectronic and chemical sensing devices. However, there is a high demand for a synthesis method that can produce large-scale and reliable high-quality $PtSe_2$. In this study, the growth of $PtSe_2$ is presented by metal–organic vapor deposition on a variety of substrates. Comprehensive Raman, X-ray photoelectron, and X-ray diffraction spectroscopy, as well as scanning tunneling microscopy characterization reveals the high quality of the deposited $PtSe_2$. Domains within the films are found to be up to several hundreds of nanometers in size, and their highly ordered crystalline structure is evident from atomic-scale measurements. Electrical characterization demonstrates improved conductivity relative to conventional synthesis methods. This study provides fundamental guidance for the scalable synthesis and implementation of high quality $PtSe_2$ layers with controllable thickness, offering a key requirement for the implementation of $PtSe_2$ in future applications.

1. Introduction

2D materials are an important pillar of current materials research. Amongst the 2D materials, layered transition metal dichalcogenides (TMDs), with the general formula MX_2 (M = Metal, X = chalcogen), offer unique and diverse electronic,[1,2] photonic,[3–5] optoelectronic[6] and sensing properties.[7,8] In this context, the noble metal dichalcogenide platinum diselenide ($PtSe_2$) distinguishes itself from most other TMDs with excellent high-stability in ambient conditions,[9,10] which makes it a prime candidate for many applications and electronic device integration.[11–15]

$PtSe_2$ has six possible crystallographic phases[16] with the 1T phase being the most commonly experimentally observed. One distinguishing feature of $PtSe_2$ is that it undergoes a semimetal-to-semiconductor transition when thinned from bulk.[17,18] As a monolayer, it displays a band gap in the infrared (IR) range[11,19] and carrier mobilities[9] amongst the highest observed for TMD materials. $PtSe_2$ has been shown to be a prime material for chemical sensing devices,[8,20] optoelectronic IR waveguide detectors[6] but it also has proven viability for use in transistors[17] and in thermoelectric devices due to its high Seebeck coefficient.[21] Nevertheless, a high-quality, large-scale, and reproducible synthesis approach for $PtSe_2$ is still highly sought after to fully exploit its unique properties in novel devices.

To date, besides exfoliation techniques,[7] a limited number of synthesis techniques for large-scale, thin $PtSe_2$ films have been reported, which mainly fall into two related categories, chemical vapor deposition[22–25] (CVD) and thermal-assisted conversion (TAC).[6,8,9,20] In TAC, pre-deposited Pt layers are converted with

M. Prechtl, S. Heiserer, M. Busch, O. Hartwig, C. Ó Coileáin, T. Stimpel-Lindner, K. Lee, G. S. Duesberg
Institute of Physics
Faculty of Electrical Engineering and Information Technology and SENS Research Centre
University of the Bundeswehr Munich
85577 Neubiberg, Germany
E-mail: duesberg@unibw.de

The ORCID identification number(s) for the author(s) of this article can be found under https://doi.org/10.1002/aelm.202400392

© 2024 The Author(s). Advanced Electronic Materials published by Wiley-VCH GmbH. This is an open access article under the terms of the Creative Commons Attribution License, which permits use, distribution and reproduction in any medium, provided the original work is properly cited.

DOI: 10.1002/aelm.202400392

K. Zhussupbekov, A. Zhussupbekova, S. Berman, I. V. Shvets
CRANN
School of Physics
Trinity College Dublin
Dublin 2, D02 PN40, Ireland

K. Zhussupbekov, A. Zhussupbekova
School of Chemistry
Trinity College Dublin
Dublin 2, D02 PN40, Ireland

Se vapor to $PtSe_2$ which can produce continuous large-scale films of controlled thickness. TAC synthesis can be performed at low temperatures, enabling synthesis even on flexible substrates.[26] Conformal and selective deposition has been reported with TAC in combination with atomic layer deposition of the Pt film.[8] However, the individual $PtSe_2$ crystallites of TAC-produced films typically have sizes of only a few nanometers,[20,26,27] which limits the fabrication of single crystal devices and the growth of monolayer films. CVD growth of $PtSe_2$ with inorganic precursors can yield monolayer individual flakes, in particular when using crystalline substrates such as sapphire or polycrystalline films over limited areas.[22–25] Ultimately controllable growth of continuous films of $PtSe_2$ on a large scale remains elusive since seeding, uniformity, and reproducibility of CVD remain as open challenges and the growth kinetics are yet to be well understood.[28,29] Hence, new growth techniques are required, with the prospects of improved material characteristics, that combine the material quality of CVD with the versatility, reproducibility, and scalability of TAC synthesis.

In this work, we introduce metal–organic (MO)CVD growth of $PtSe_2$ as a highly reproducible synthesis route. MOCVD combines vaporized $C_9H_{16}Pt$ as a platinum precursor and evaporated Se under H_2 carrier flow as selenium source to achieve scalable growth of high-quality $PtSe_2$ layers on a variety of commonly used substrates such SiO_2, *c*-plane sapphire, and pyrolytic carbon (PyC). A custom-built synthesis setup fully encapsulated in a glovebox was used for the $PtSe_2$ growth, allowing versatile and safe growth on large areas, accommodating up to 6-inch wafers. The characteristics of the grown films were evaluated using Raman spectroscopy, X-ray photoelectron spectroscopy (XPS), atomic force microscopy (AFM), and X-ray diffraction spectroscopy (XRD), which consistently demonstrated high material quality. Furthermore, the atomic and electronic structure of the deposited layers is investigated by scanning tunneling microscopy (STM) and spectroscopy (STS), which revealed domain sizes within the layers of up to 300 nm. These domains were found to have large areas of defect-free growth, as observed in STM measurements. Finally, an etching process was developed, and a transfer length method (TLM) was performed, which indicated the good electrical performance of the MOCVD-synthesized $PtSe_2$. The electrical results demonstrated improved conductivity over TAC-derived films. This work provides a synthesis and integration route for high-quality, large-scale $PtSe_2$ layers, laying a cornerstone for the integration of $PtSe_2$ into novel devices.

2. Results and Discussion

2.1. Scalable Synthesis of $PtSe_2$ on Various Substrates

$PtSe_2$ films were synthesized by MOCVD in a custom-built cold-wall reactor shown in **Figure 1a**. The key components of the low-pressure growth chamber and the gas flow directions during deposition are sketched in Figure 1b. The sample substrates are placed on a 6-inch substrate plate. H_2 is allowed to flow over heated selenium powder (225 °C), serving as a chalcogen precursor. The metal–organic $C_9H_{16}Pt$ platinum precursor heated to 40 °C and supplied through heated pipes. Prior to deposition, the substrates are typically annealed under an H_2 flow for 15 min at 600 °C. The temperature was kept at 600 °C during growth. All parameters used are carefully optimized to ensure reproducible growth of high-quality $PtSe_2$.[30] Homogenous deposition was achieved on 1 × 1 cm^2 *c*-plane sapphire (Figure 1c) and SiO_2 (Figure 1d) substrates. Additional scanning electron microscopy images of deposited layers can be found in Figure S1 (Supporting Information).

The growth method allows fine control of film thickness by adjusting the growth duration. It is noteworthy that the process time for MOCVD-grown thin films is significantly shorter than for conventional TAC processes.[20,26,27] The growth rates (GRs) on different substrates were determined by subsequent AFM measurements (Figure 1e,f) and were found to be $GR\ (sapphire) = 1.2\ \frac{nm}{min}$ for *c*-plane sapphire (Figure 1g) substrates and $GR\ (SiO_2) = 1.0\ \frac{nm}{min}$ for SiO_2 substrates (Figure 1h). Notably, the growth rate is slightly higher on crystalline *c*-plane sapphire compared to amorphous SiO_2. The intercepts with the *x*-axis of the linear fits indicate the time need for seeding and are found to be similar at ≈129 and 120 s for *c*-plane sapphire and SiO_2, respectively. However, looking at growth times close to this limit, no $PtSe_2$ growth was observed by either Raman or AFM measurements on the SiO_2 surface for a deposition time of 110 s, a time which already resulted in a ≈1 nm thick film on *c*-plane sapphire. This indicates that the first layers are formed faster on the *c*-plane sapphire than on the amorphous SiO_2. The root mean square roughness values derived from AFM measurements are lower for $PtSe_2$ films on sapphire than on SiO_2, suggesting better planar alignment and more efficient nucleation on the crystalline substrate (see Figure S2, Supporting Information). These influences on growth dynamics are consistent with the CVD of other TMD materials due to the different surface energy and morphology of the substrates.[31,32]

2.2. Layer Quality Analysis by Raman Spectroscopy, XPS, and XRD Measurements

To investigate the material quality, Raman spectra were acquired for $PtSe_2$ layers of different thicknesses grown on *c*-plane sapphire substrates. The spectra were averaged over a total of 100 measurement points distributed over the whole samples to increase statistical significance (**Figure 2a**). A detailed Raman analysis for $PtSe_2$ grown on SiO_2 substrates can be found in the Supporting Information. For all spectra, the fundamental $PtSe_2$ fingerprint E_g and A_{1g} modes can be identified, while also a prominent interlayer mode located at 24 cm^{-1} is present in the spectrum of the 1 nm $PtSe_2$ (black). The absence of the interlayer mode for thicker layers is expected as it becomes less prominent for increasing film thickness.[33] The evolution of the peak center position and FWHM for the E_g and A_{1g} modes are shown in Figure 2b. For the E_g (A_{1g}) mode a redshift from 181.07 cm^{-1} (208.62 cm^{-1}) to 178.2 cm^{-1} (206.54 cm^{-1}) is observed with increased thickness, and is consistent with other reports on the growth $PtSe_2$ and TMD materials.[33–35] The FWHM of the E_g mode, which is directly correlated to layer quality,[35,36] ranges from 4.3 to 5.6 cm^{-1}, indicating high layer quality.[35] However, the highest FWHM from the 46 nm thick film indicates an increasing variance of crystallite thickness and correlates with increased roughness of the thickest film. The XRD

© 2024 The Author(s). Advanced Electronic Materials published by Wiley-VCH GmbH
2199160x, 0, Downloaded from https://onlinelibrary.wiley.com/doi/10.1002/aelm.202400392 by Universitat der Bundeswehr Munchen, Wiley Online Library on [24/01/2025]. See the Terms and Conditions (https://onlinelibrary.wiley.com/terms-and-conditions) on Wiley Online Library for rules of use; OA articles are governed by the applicable Creative Commons License

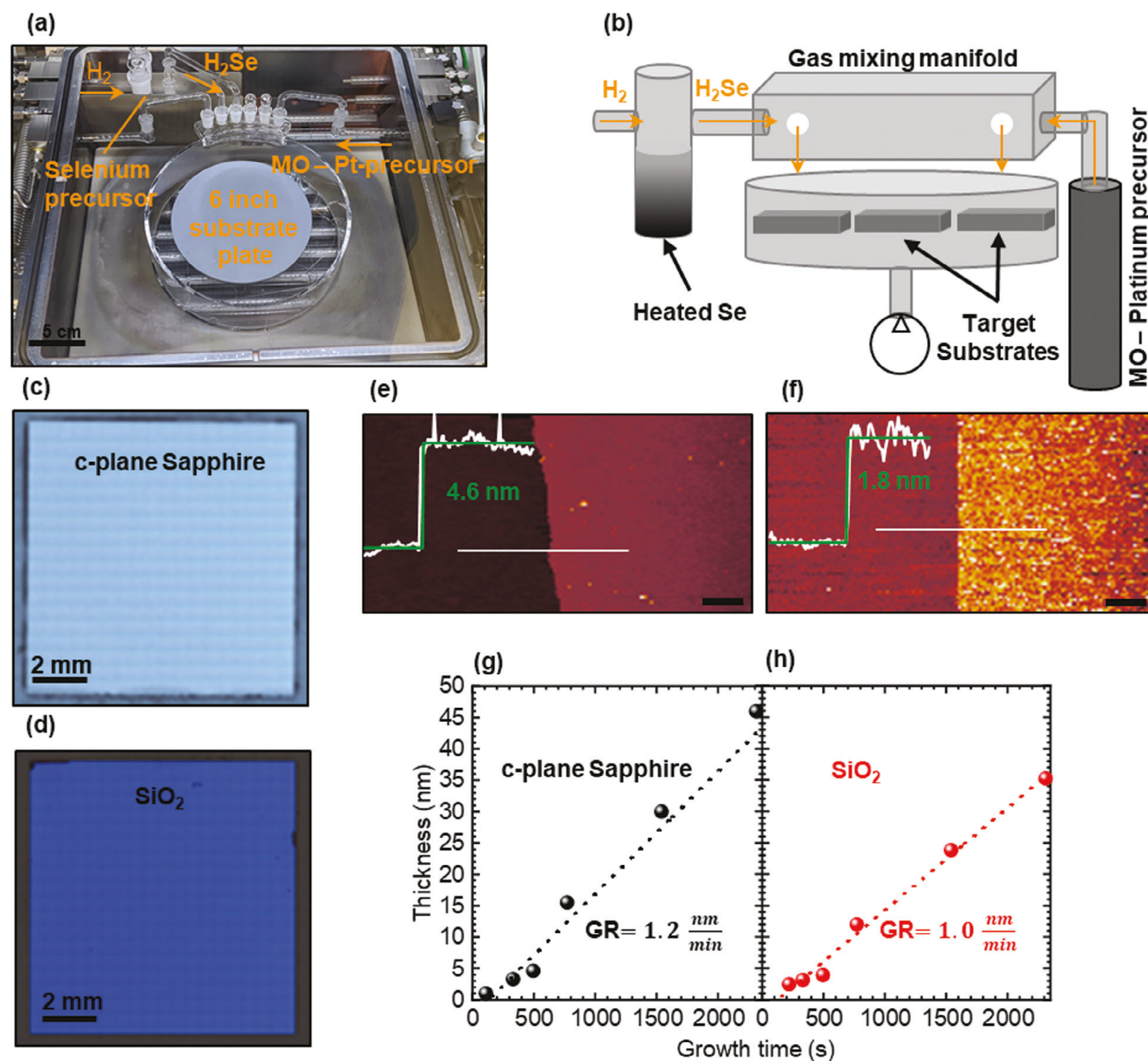

Figure 1. Synthesis of $PtSe_2$ by MOCVD. a) Photograph of the 6″ custom-built MOCVD reactor. b) Schematic of the reactor chamber. c) 1 nm and d) 3.2 nm $PtSe_2$ layer homogenously deposited on 1 × 1 cm^2 scale c) *c*-plane sapphire and d) SiO_2 substrates. e) AFM image including height profile (white) and fit (green) for 4.6 nm thick $PtSe_2$ grown on *c*-plane sapphire and f) 1.8 nm $PtSe_2$ grown on SiO_2, profile positions are marked as white lines. The scale bars (black) are 1 µm. g,h) $PtSe_2$ layer thickness versus growth time on *c*-plane sapphire and SiO_2, respectively. Growth rates (GR) have been calculated from linear fits (dashed lines).

pattern (Figure 2c) shows a strong feature at 17.3° which can be attributed to the (001) plane of $PtSe_2$[36,37] and suggests planar alignment of the crystallites.[38] The presence of further peaks (inset) from higher-index planes of $PtSe_2$[39] shows the high crystallinity of the material. For chemical binding analysis of the synthesized $PtSe_2$, spectra of the core level binding energies of the Pt4f (Figure 2d) and Se3d (Figure 2e) regions are acquired by XPS measurements. The signal acquired from the Pt4f peak (grey) region consists of three peaks. The main contribution (blue) has its maximum at 73.3 eV and indicates that 90% of the Pt is present in the form of $PtSe_2$. About 6.8% (red) of the signal contribution stems from Pt-atoms present in a sub-stochiometric form $PtSe_x$. The remaining 3.2% (green) are found in a slightly higher binding state which is tentatively attributed to surface oxidation. Sufficient fitting of the Pt4f spectrum can also be achieved without incorporating an oxidized Pt species, by using asymmetrical peak shapes due to the semi-metallic property of $PtSe_2$.[40] The latter two contributions are mainly present on the surface of the films, where a loss of selenium atoms ($PtSe_x$), and consequently oxidation (PtO_x) is expected.[41] The raw signal of the Se3d core level region (Figure 2e, grey) consists of three doublets and a singlet. The main contribution, with 88.2% (blue), originates from $PtSe_2$, while 1.7% and 10.1% are attributed to $PtSe_x$ and SeO_x, respectively. The last contribution (purple) stems from the $Pt5p_{3/2}$ orbital and was not taken into account when calculating the $PtSe_2$ stoichiometric ratio of 1:1.83.

© 2024 The Author(s). Advanced Electronic Materials published by Wiley-VCH GmbH

2199160x, 0, Downloaded from https://onlinelibrary.wiley.com/doi/10.1002/aelm.202400392 by Universitat der Bundeswehr Munchen, Wiley Online Library on [24/01/2025]. See the Terms and Conditions (https://onlinelibrary.wiley.com/terms-and-conditions) on Wiley Online Library for rules of use; OA articles are governed by the applicable Creative Commons License

2199160x, 0, Downloaded from https://onlinelibrary.wiley.com/doi/10.1002/aelm.202400392 by Universitat der Bundeswehr Munchen, Wiley Online Library on [24/01/2025]. See the Terms and Conditions (https://onlinelibrary.wiley.com/terms-and-conditions) on Wiley Online Library for rules of use; OA articles are governed by the applicable Creative Commons License

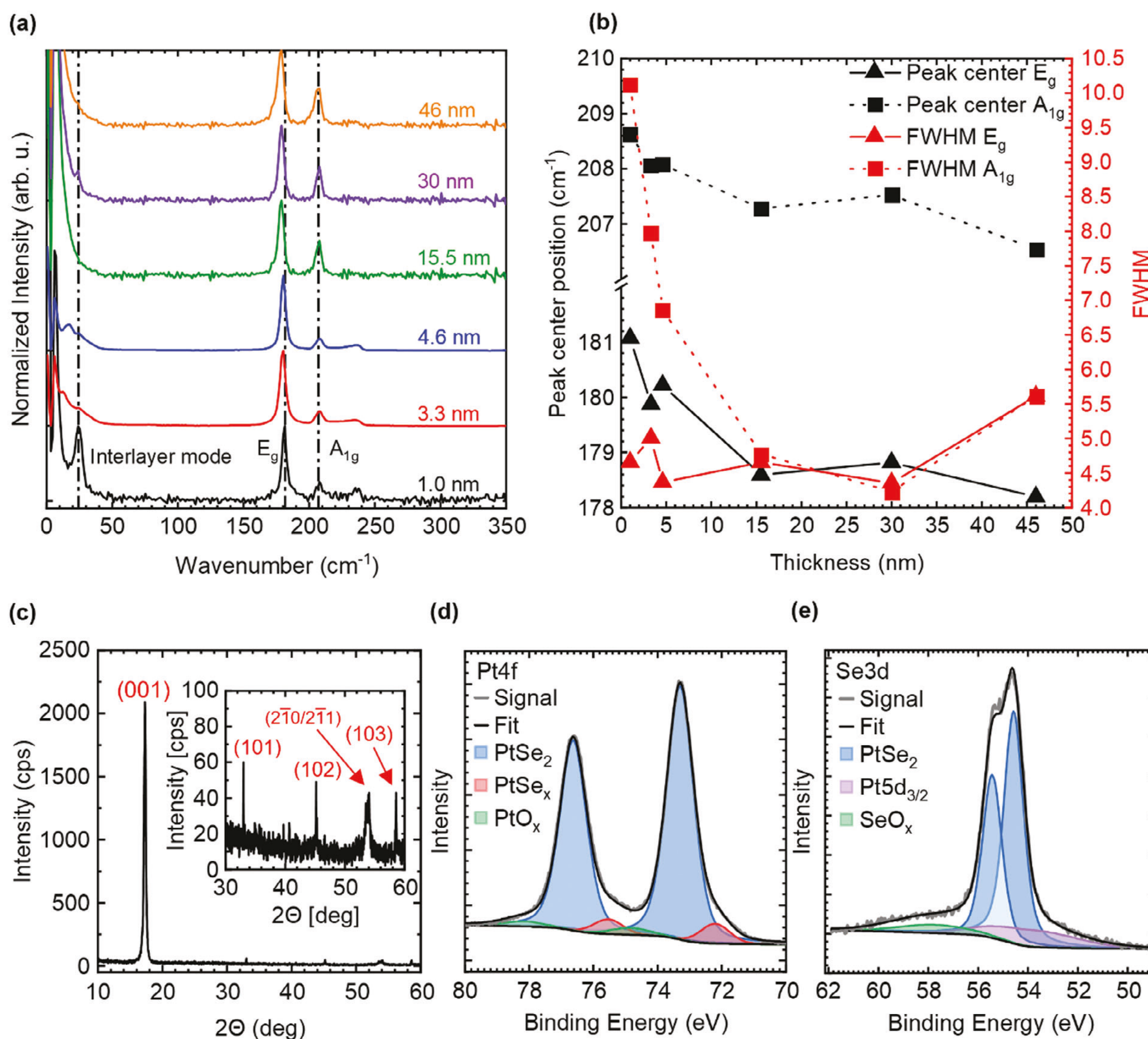

Figure 2. Raman spectra, XRD, and XPS analysis of MOCVD grown $PtSe_2$. a) Normalized, averaged Raman spectra of different thickness $PtSe_2$ films grown on *c*-plane sapphire. b) Peak center of the E_g (black triangle) and A_{1g} (black square) mode and respective FWHM (red) for different thickness $PtSe_2$ films. c) XRD pattern of a 35 nm thick $PtSe_2$ film. Inset showing a magnification of the same plot. XPS of the Pt4f core level region (d) and Se3d core level region (e). The spectra have been fitted to highlight the individual contributions to the raw signal (grey).

Furthermore, the survey spectrum (see Figure S4, Supporting Information) did not show any significant other chemical components in our sample. In summary, detailed Raman analysis and XRD measurements confirm the high-quality growth of $PtSe_2$ by our newly developed MOCVD approach. In addition, XPS measurements support the conclusions drawn from Raman and XRD analysis.

2.3. Structural and Electronic Investigation by Atomically Resolved STM and STS Measurements

The atomic structure and local density of states of the $PtSe_2$ were examined with STM (**Figure** 3a,b,d) and STS (Figure 3c). Single-crystalline $PtSe_2$ domains with sizes of 50 to 300 nm could be identified in large-scale STM and SEM images, as shown in Figure 3a and Figure S1c (Supporting Information). Although at smaller scales some contamination is visible, likely from ex situ transfer, large uniform terraces can be observed (Figure 3b). STS measurements and STM at a number of bias voltages were performed within the region outlined by the black dash square in Figure 3b. As illustrated in Figure 3c, the plot of conductivity (dI/dV) evinces the semimetallic character of the ≈35 nm thick $PtSe_2$ film. Despite the reduced density of states near zero bias, there is no discernible gap opening, indicating that the film possesses semimetallic properties.[42] This result is consistent with previous reports of semimetallic behavior in $PtSe_2$ films of this thickness.[43–45] Furthermore, atomically resolved STM images (Figure 3d; Figure S5, Supporting Information) show an ordered $PtSe_2$ lattice without any visible defects, once again substantiating the high quality of $PtSe_2$ by our newly developed MOCVD approach.

© 2024 The Author(s). Advanced Electronic Materials published by Wiley-VCH GmbH

2199160x, 0, Downloaded from https://onlinelibrary.wiley.com/doi/10.1002/aelm.202400392 by Universitat der Bundeswehr Munchen, Wiley Online Library on [24/01/2025]. See the Terms and Conditions (https://onlinelibrary.wiley.com/terms-and-conditions) on Wiley Online Library for rules of use; OA articles are governed by the applicable Creative Commons License

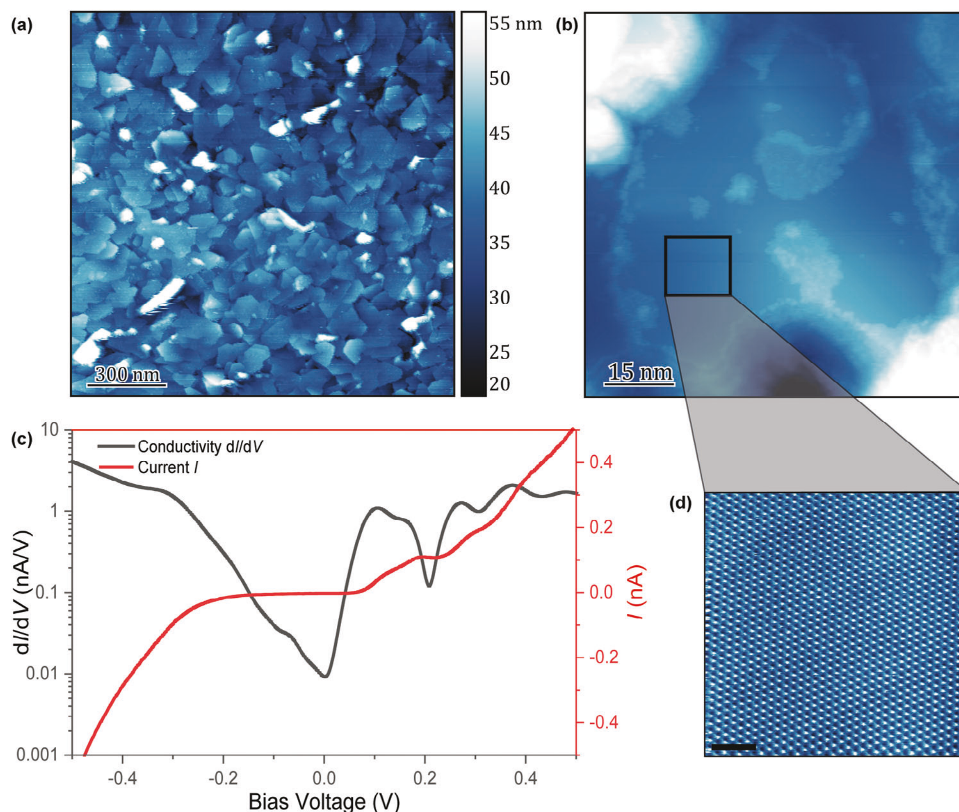

Figure 3. STM and STS of a 35 nm thick $PtSe_2$ film on PyC. a) Large-scale STM image of $PtSe_2$ grown on PyC ($V = 2.8$ V, $I = 70$ pA, 1500×1500 nm^2). Domain sizes in the range of 50 to 300 nm are visible. The black dash square in (b) ($V = 2.8$ V, $I = 90$ pA, 85×85 nm^2) indicates the area where the STS measurement has been conducted and the atomic resolution image obtained. c) Derivative of current (black) and current (red) dependent on bias voltage used in STS. d) Atomically resolved structure of $PtSe_2$ obtained at −0.4 V bias voltages. The scale bar is 2 nm, the total size of the scan is 13×13 nm^2. Images at other bias voltages are displayed in Figure S5 (Supporting Information).

2.4. Device Fabrication and Electrical Characterization of MOCVD-Grown $PtSe_2$

Large-scale $PtSe_2$ thin films would have potential applications for devices such field effect transistors,[9] gas sensors,[20] or optical waveguides.[6,8] However, to realize these applications it is necessary to structure such large-area films. Even though selective synthesis of $PtSe_2$ is a possible fabrication route,[8] it is more viable to structure the $PtSe_2$ after synthesis when MOCVD is used. Consequently, we developed a dry-etching process using reactive ion etching (RIE) to structure the as-grown $PtSe_2$ layers. A lithographically structured photoresist was used to define and protect channel regions and a combination of SF_6 and oxygen plasma was used to etch the $PtSe_2$ at a rate of ≈2 nm min^{-1}, allowing a precise etching. In a second lithography step, Ni/Au contacts were deposited with a variety of separations to define different channel lengths. This method was applied to films with a variety of thicknesses to electrically characterize the $PtSe_2$ using the transfer length method (TLM).[35]

Figure 4a shows the drain current I_d versus the applied voltage V_d for different channel lengths for a 100 µm wide and 9.2 nm thick MOCVD-grown $PtSe_2$ film. The measured resistances and corresponding channel lengths were plotted and a linear fit was applied, yielding an adjusted R^2 of 0.998 (Figure 4b). A sheet resistance (R_S) of 4.7 kΩ sq^{-1} and a contact resistance (R_C) of 0.3 kΩ were derived from the slope and y-intercept, respectively. The output characteristics of all MOCVD-grown samples are displayed in Figure S6 (Supporting Information). Notably, the conductivities of the MOCVD-grown $PtSe_2$ films exceed the values determined for films of equivalent thickness prepared by the TAC process by more than an order of magnitude (Figure 4c), also when compared to previously reported $PtSe_2$ synthesized by TAC using standard parameters.[35] Details on the processes are described in the Experimental Section. The electrical conductivity of MOCVD-grown $PtSe_2$ is superior to that of TAC-grown materials due to larger grain size, improved homogeneity, and enhanced crystallinity.[36] This aligns with structural analysis outcomes and provides evidence of the superior quality of the material synthesized using our newly developed technique.

3. Conclusion

$PtSe_2$ was grown by combining an MO platinum and a selenium precursor source. Centimeter-scale synthesis was shown on SiO_2, c-plane sapphire, and PyC substrates. The high quality of the synthesized material was verified by Raman, XPS, and XRD measurements. Atomically resolved STM measurements revealed hexagonal $PtSe_2$ single crystals up to 300 nm in size. In addition, STM images confirmed the low defect concentration and highly ordered nature of the crystallites, demonstrating the

© 2024 The Author(s). Advanced Electronic Materials published by Wiley-VCH GmbH

2199160x, 0, Downloaded from https://onlinelibrary.wiley.com/doi/10.1002/aelm.202400392 by Universitat der Bundeswehr Munchen, Wiley Online Library on [24/01/2025]. See the Terms and Conditions (https://onlinelibrary.wiley.com/terms-and-conditions) on Wiley Online Library for rules of use; OA articles are governed by the applicable Creative Commons License

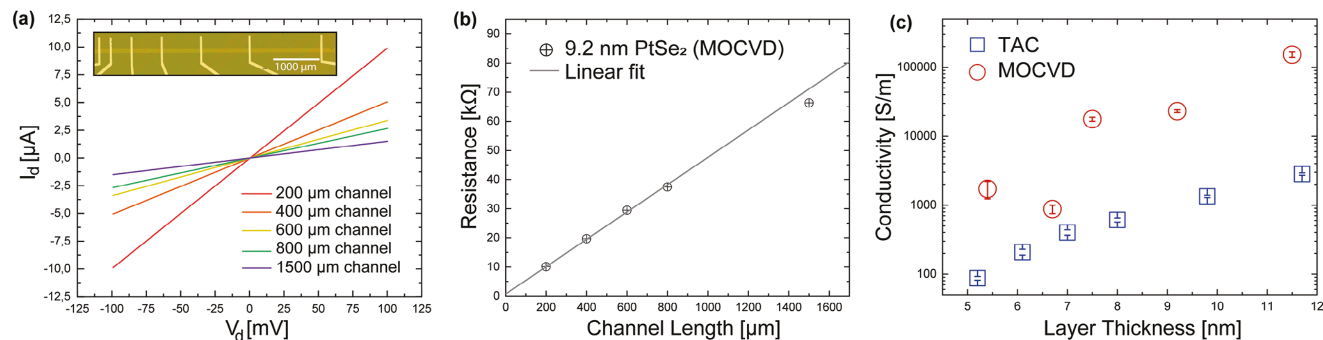

Figure 4. Sheet resistance from TLM measurements. a) Output characteristics (I_d–V_d curves) of 9.2 nm thick MOCVD-grown $PtSe_2$ for a 100 µm wide channel with various channel lengths. The channel was defined by the RIE of the MOCVD $PtSe_2$ followed by subsequent deposition of metal contacts. Inset: an optical image of the TLM structure. b) Resistance versus channel length for 9.2 nm MOCVD-grown $PtSe_2$, with linear fit showing resistance is proportionally dependent to channel length. c) Conductivities of $PtSe_2$ films of different thicknesses grown by TAC (blue squares) and MOCVD (red circles). For all thicknesses, the MOCVD-grown material is observed to have higher electrical conductivity.

high quality of the material. The superior electrical conductivity of MOCVD-grown material compared to TAC-grown films of similar thickness aligns with the outcomes of structural analysis and demonstrates the advantage of our newly developed method. Additionally, the study demonstrates successful growth in a 6′′ wafer tool, paving the way toward industrial-scale synthesis of $PtSe_2$ and its future implementation into real-world devices.

4. Experimental Section

MOCVD Growth of $PtSe_2$: The various sample substrates were placed on the 6-inch substrate plate within the custom-built cold-wall reactor sketched in Figure 1b. Se powder (VWR, > 99.9% purity) was evaporated at 225 °C and carried by a 100sccm H_2 flow towards the reaction chamber, partially converting to H_2Se. The metal–organic platinum precursor (Trimethyl)methylcyclopentadienylplatinum(IV) $(CH_3)_3(CH_3C_5H_4)Pt$ (Strem Chemicals, 99% purity), provided in a Swagelok cylinder, was externally heated to 40 °C and supplied through heated pipes via diffusion from the heated container into the chamber. The material flux into the reaction chamber could be set via a needle valve in the connecting piping or by adjusting the precursor temperature. Prior to deposition, the substrates were typically annealed under a H_2 flow for 15 min at 600 °C. The growth of the $PtSe_2$ was typically carried out at 600 °C under low-pressure conditions.

TAC Synthesis of $PtSe_2$: For comparison of the electrical performance, $PtSe_2$ samples were synthesized using the standard TAC method.[20,34,46] SiO_2 substrates were sputter-coated with Pt thin films of varying thicknesses using a 108auto sputter coater from Cressington. Consecutively, the platinum films were converted into $PtSe_2$ under Se atmosphere at 450 °C for 120 minutes.

Growth Substrates: Successful MOCVD growth of $PtSe_2$ was shown on SiO_2, *c*-plane sapphire substrates, and PyC. PyC was used as a conductive substrate for STM/STS measurements. For electrical characterization, $PtSe_2$ films were synthesized on Si/SiO_2, which was thermally grown on Si wafers in a calibrated wet oxidation process.

AFM Analysis: A Jupiter XR AFM in tapping mode was used for the acquisition of AFM data within this study. OMCL-AC160TS tips were used in tapping mode, the tapping frequency was set in between 200 to 400 kHz. Processing of the acquired raw data and extraction of topographical information was performed using Gwyddion 2.60 (64bit).

Characterization by Raman and X-Ray Photoelectron Spectroscopy: Raman data were acquired with a WITec Alpha 300 confocal Raman system. For all measurements, a green laser (532 nm) with a power of 2 mW was used with a 100x objective (NA = 0.9). A grating with 1800 grooves per mm was used. All Raman data shown were averaged over 100 acquisition points from a 1 × 1 cm² $PtSe_2$ film. The data was analyzed and processed using the software provided with the instrument. XPS was performed on a Versa Probe XPS tool (Physical Electronics GmbH) using the monochromated Al Kα line (1486.7 eV). Single spectra were acquired at 61.8 W beam power with a 100 µm spot size. The core-level region of the C1s peak was recorded as a reference to account for any residual surface charge not compensated by the tool's built-in neutralization. Spectra were fitted with Gaussian–Lorentzian fit functions using Multi-Pak.

X-Ray Diffraction: High-resolution XRD analysis was obtained using Bruker D8 Discover equipment with a monochromated Cu Kα source.

Scanning Tunneling Microscopy and Spectroscopy: STM and STS measurements were conducted on a low-temperature microscope (Createc) at liquid nitrogen temperature (77 K). The base pressure in the main STM chamber was 5×10^{-11} mbar. Data were obtained in constant current mode using a single-crystalline W(001) tip.

Device Fabrication: To structure the MOCVD-grown $PtSe_2$ for device fabrication, a 100 µm wide channel was covered with nLOF 2070 resist using optical lithography. Subsequently, the uncovered area was etched using RIE at 850 W plasma power and 100 pa pressure with 100 sccm SF_6 200 sccm O_2 supply. For TAC-synthesized samples, Pt channels were pre-structured before conversion using optical lithography.

Electrical Characterization: Electrical measurements were performed using TLM. The $PtSe_2$ on Si/SiO_2 was structured into a 100 µm wide channel and Ni/Au contacts were deposited by evaporation, spaced 200 µm, 400 µm, 600 µm, 800 µm, and 1500 µm apart, defining the respective channel length. The resistance $R = \frac{\partial I_d}{\partial V_d}$ was derived using a linear fit of the I_d–V_d curve shown in Figure 4a. The sheet resistance $R_S = \frac{\partial R}{\partial l} \times w$ was derived from the slope of the linear fit in Figure 4b and the channel width w = 100 µm. The *y*-intercept corresponds to $2R_C$.

Supporting Information

Supporting Information is available from the Wiley Online Library or from the author.

Acknowledgements

This work was financially supported by the European Commission under the projects ULISSES [825272], QUEFORMAL [829035], and Graphene Flagship [881603], as well as the German Ministry of Education and Research (BMBF) under the projects NobleNEMS [16ES1121] and ACDC [13N15100]. Further, the authors thank dtec.bw—Digitalization and Technology Research Center of the Bundeswehr for support (project VITAL-SENSE). dtec.bw was funded via the German Recovery and Resilience Plan

 © 2024 The Author(s). Advanced Electronic Materials published by Wiley-VCH GmbH

by the European Union (NextGenerationEU). K.Z. and A.Z. would also like to acknowledge IRC funding through awards GOIPD/2022/774 and GOIPD/2022/443.

Conflict of Interest

The authors declare no conflict of interest.

Author Contributions

M.P. and S.H. contributed equally to this work. M.P., S.H., C.Ó., and G.S.D. conceived and defined the study. G.S.D and I.V.S. supervised the study. M.P., S.H., and M.B. synthesized the material and conducted Raman and AFM measurements. A.Z. conducted XRD measurements and analyzed the data. O.H. conducted XPS measurements and analyzed the spectra by multiple peak fitting. K.Z. and S.B. acquired STM and STS images, C.Ó., K.Z., and I.V.S. analyzed the respective data. S.H. and K.L. fabricated the devices and performed electrical characterization. All authors extensively discussed and reviewed the manuscript. M.P., S.H., C.Ó., and G.S.D. wrote the manuscript with input from all authors.

Data Availability Statement

The data that support the findings of this study are available from the corresponding author upon reasonable request.

Keywords

2D material synthesis, metal–organic chemical vapor deposition MOCVD, platinum diselenide $PtSe_2$, sensor material, transition metal dichalcogenides TMD

Received: May 15, 2024
Revised: August 23, 2024
Published online:

[1] M. C. Lemme, D. Akinwande, C. Huyghebaert, C. Stampfer, *Nat. Commun.* **2022**, *13*, 1392.
[2] G. Fiori, F. Bonaccorso, G. Iannaccone, T. Palacios, D. Neumaier, A. Seabaugh, S. K. Banerjee, L. Colombo, *Nat. Nanotechnol.* **2014**, *9*, 768.
[3] M. Turunen, M. Brotons-Gisbert, Y. Dai, Y. Wang, E. Scerri, C. Bonato, K. D. Jöns, Z. Sun, B. D. Gerardot, *Nat. Rev. Phys.* **2022**, *4*, 219.
[4] A. D. Alfieri, M. J. Motala, M. Snure, J. Lynch, P. Kumar, H. Zhang, S. Post, T. Bowen, C. Muratore, J. A. Robinson, J. R. Hendrickson, N. R. Glavin, D. Jariwala, *Adv. Opt. Mater.* **2023**, *11*, 2202011.
[5] G. A. Ermolaev, K. V. Voronin, M. K. Tatmyshevskiy, A. B. Mazitov, A. S. Slavich, D. I. Yakubovsky, A. P. Tselin, M. S. Mironov, R. I. Romanov, A. M. Markeev, I. A. Kruglov, S. M. Novikov, A. A. Vyshnevyy, A. V. Arsenin, V. S. Volkov, *Nanomaterials* **2021**, *11*, 3269.
[6] S. Parhizkar, M. Prechtl, A. L. Giesecke, S. Suckow, S. Wahl, S. Lukas, O. Hartwig, N. Negm, A. Quellmalz, K. Gylfason, D. Schall, M. Wuttig, G. S. Duesberg, M. C. Lemme, *ACS Photonics* **2022**, *9*, 859.
[7] K. Lee, B. M. Szydlowska, O. Hartwig, K. Synnatschke, B. Tywoniuk, T. Hartman, T. Tomasevic-Ilic, C. P. Gabbett, J. N. Coleman, Z. Sofer, M. Spasenovic, C. Backes, G. S. Duesberg, *J. Mater. Chem. C* **2023**, *11*, 593.
[8] M. Prechtl, S. Parhizkar, O. Hartwig, K. Lee, J. Biba, T. Stimpel-Lindner, F. Gity, A. Schels, J. Bolten, S. Suckow, A. L. Giesecke, M. C. Lemme, G. S. Duesberg, *Adv. Funct. Mater.* **2021**, *31*, 2103936.
[9] Y. Zhao, J. Qiao, Z. Yu, P. Yu, K. Xu, S. P. Lau, W. Zhou, Z. Liu, X. Wang, W. Ji, Y. Chai, *Adv. Mater.* **2017**, *29*, 1604230.
[10] A. A. Puretzky, A. D. Oyedele, K. Xiao, A. V. Haglund, B. G. Sumpter, D. Mandrus, D. B. Geohegan, L. Liang, *2D Mater.* **2018**, *5*, 35016.
[11] L. Ansari, S. Monaghan, N. McEvoy, C. Ó. Coileáin, C. P. Cullen, J. Lin, R. Siris, T. Stimpel-Lindner, K. F. Burke, G. Mirabelli, R. Duffy, E. Caruso, R. E. Nagle, G. S. Duesberg, P. K. Hurley, F. Gity, *npj 2D Mater. Appl.* **2019**, *3*, 33.
[12] W. Xu, J. Jiang, H. Ma, Z. Zhang, J. Li, B. Zhao, R. Wu, X. Yang, H. Zhang, B. Li, W. Shu, Z. Zhang, B. Li, Y. Liu, L. Liao, X. Duan, *Nano Res.* **2020**, *13*, 2091.
[13] A. Avsar, C. Y. Cheon, M. Pizzochero, M. Tripathi, A. Ciarrocchi, O. V. Yazyev, A. Kis, *Nat. Commun.* **2020**, *11*, 4806.
[14] D. Qin, P. Yan, G. Ding, X. Ge, H. Song, G. Gao, *Sci. Rep.* **2018**, *8*, 2764.
[15] M. Wei, J. Lian, Y. Zhang, C. Wang, Y. Wang, Z. Xu, *npj 2D Mater. Appl.* **2022**, *6*, 1.
[16] R. Kempt, S. Lukas, O. Hartwig, M. Prechtl, A. Kuc, T. Brumme, S. Li, D. Neumaier, M. C. Lemme, G. S. Duesberg, T. Heine, *Adv. Sci.* **2022**, *9*, 2201272.
[17] A. Ciarrocchi, A. Avsar, D. Ovchinnikov, A. Kis, *Nat. Commun.* **2018**, *9*, 919.
[18] W. Zhang, J. Qin, Z. Huang, W. Zhang, *J. Appl. Phys.* **2017**, *122*, 205701.
[19] C. Yim, N. McEvoy, S. Riazimehr, D. S. Schneider, F. Gity, S. Monaghan, P. K. Hurley, M. C. Lemme, G. S. Duesberg, *Nano Lett.* **2018**, *18*, 1794.
[20] C. Yim, K. Lee, N. McEvoy, M. O'Brien, S. Riazimehr, N. C. Berner, C. P. Cullen, J. Kotakoski, J. C. Meyer, M. C. Lemme, G. S. Duesberg, *ACS Nano* **2016**, *10*, 9550.
[21] G. S. Kim, N.-W. Park, M. S. Kang, J. W. Choi, W. Y. Lee, S. K. Lee, *J. Phys. Chem. C* **2022**, *126*, 4150.
[22] Z. Wang, Q. Li, F. Besenbacher, M. Dong, *Adv. Mater.* **2016**, *28*, 10224.
[23] X. Yu, P. Yu, W. Di, B. Singh, Q. Zeng, H. Lin, W. Zhou, J. Lin, K. Suenaga, Z. Liu, Q. J. Wang, *Nat. Commun.* **2018**, *9*, 1545.
[24] H. Xu, H. Zhang, Y. Liu, S. Zhang, Y. Sun, Z. Guo, Y. Sheng, X. Wang, C. Luo, X. Wu, J. Wang, W. Hu, Z. Xu, Q. Sun, P. Zhou, J. Shi, Z. Sun, D. W. Zhang, W. Bao, *Adv. Funct. Mater.* **2018**, *306*, 1805614.
[25] J. Xie, D. Zhang, X. Q. Yan, M. Ren, X. Zhao, F. Liu, R. Sun, X. Li, Z. Li, S. Chen, Z.-B. Liu, J. G. Tian, *2D Mater.* **2019**, *6*, 35011.
[26] C. S. Boland, C. Ó. Coileáin, S. Wagner, J. B. McManus, C. P. Cullen, M. C. Lemme, G. S. Duesberg, N. McEvoy, *2D Mater.* **2019**, *6*, 45029.
[27] S. Wagner, C. Yim, N. McEvoy, S. Kataria, V. Yokaribas, A. Kuc, S. Pindl, C. P. Fritzen, T. Heine, G. S. Duesberg, M. C. Lemme, *Nano Lett.* **2018**, *18*, 3738.
[28] J. Zhang, T. Zhai, F. Arifurrahman, Y. Wang, A. Hitt, Z. He, Q. Ai, Y. Liu, C. Y. Lin, Y. Zhu, M. Tang, J. Lou, *Nano Lett.* **2024**, *24*, 2465.
[29] Y. Gong, J. Lin, X. Wang, G. Shi, S. Lei, Z. Lin, X. Zou, G. Ye, R. Vajtai, B. I. Yakobson, H. Terrones, M. Terrones, B. K. Tay, J. Lou, S. T. Pantelides, Z. Liu, W. Zhou, P. M. Ajayan, *Nat. Mater.* **2014**, *13*, 1135.
[30] S. Heiserer, P. Eder, C. Ó. Coileáin, J. Biba, T. Stimpel-Lindner, C. Bartlam, U. Rührmair, G. S. Duesberg, *Adv. Electron. Mater.* **2023**, *9*, 2300281.
[31] T. Han, H. Liu, S. Wang, S. Chen, W. Li, X. Yang, M. Cai, K. Yang, *Nanomaterials* **2019**, *9*, 740.
[32] L. Peters, C. ÓCoileáin, P. Dluzynski, R. Siris, G. S. Duesberg, N. McEvoy, *Phys. Status Solidi (A)* **2020**, *217*, 2000073.
[33] X. Chen, S. Zhang, L. Wang, Y.-F. Huang, H. Liu, J. Huang, N. Dong, W. Liu, I. M. Kislyakov, J. M. Nunzi, L. Zhang, J. Wang, *Photonics Res.* **2019**, *7*, 1416.
[34] M. O'Brien, N. McEvoy, C. Motta, J.-Y. Zheng, N. C. Berner, J. Kotakoski, K. Elibol, T. J. Pennycook, J. C. Meyer, C. Yim, M. Abid, T. Hallam, J. F. Donegan, S. Sanvito, G. S. Duesberg, *2D Mater.* **2016**, *3*, 21004.

© 2024 The Author(s). Advanced Electronic Materials published by Wiley-VCH GmbH

2199160x, 0, Downloaded from https://onlinelibrary.wiley.com/doi/10.1002/aelm.202400392 by Universitat der Bundeswehr Munchen, Wiley Online Library on [24/01/2025]. See the Terms and Conditions (https://onlinelibrary.wiley.com/terms-and-conditions) on Wiley Online Library for rules of use; OA articles are governed by the applicable Creative Commons License

[35] S. Lukas, O. Hartwig, M. Prechtl, G. Capraro, J. Bolten, A. Meledin, J. Mayer, D. Neumaier, S. Kataria, G. S. Duesberg, M. C. Lemme, *Adv. Funct. Mater.* **2021**, *31*, 2102929.
[36] W. Jiang, X. Wang, Y. Chen, G. Wu, K. Ba, N. Xuan, Y. Sun, P. Gong, J. Bao, H. Shen, T. Lin, X. Meng, J. Wang, Z. Sun, *InfoMat* **2019**, *1*, 260.
[37] L. Zeng, S. Lin, Z. Lou, H. Yuan, H. Long, Y. Li, W. Lu, S. P. Lau, D. Wu, Y. H. Tsang, *npg Asia Mater.* **2018**, *10*, 352.
[38] M. Sojková, J. Hrdá, S. Volkov, K. Vegso, A. Shaji, T. Vojteková, L. P. Slusná, N. Gál, E. Dobrocka, P. Siffalovic, T. Roch, M. Gregor, M. Hulman, *Appl. Phys. Lett.* **2021**, *119*, 013101.
[39] The Materials Project, Materials Data on PtSe2 (mp-1115), **2020**, https://doi.org/10.17188/1187595.
[40] A. Enrico, O. Hartwig, N. Dominik, A. Quellmalz, K. B. Gylfason, G. S. Duesberg, F. Niklaus, G. Stemme, *ACS Nano* **2023**, *17*, 8041.
[41] J. B. McManus, D. V. Horvath, M. P. Browne, C. P. Cullen, G. Cunningham, T. Hallam, K. Zhussupbekov, D. Mullarkey, C. Ó. Coileáin, I. V. Shvets, M. Pumera, G. S. Duesberg, N. McEvoy, *Nanotechnology* **2020**, *31*, 375601.
[42] K. Zhussupbekov, L. Ansari, K. Elibol, A. Zhussupbekova, J. Kotakoski, I. V. Shvets, G. S. Duesberg, P. K. Hurley, N. McEvoy, C. Ó. Coileáin, F. Gity, *Appl. Mater. Today* **2023**, *35*, 101926.
[43] J. Li, S. Kolekar, Y. Xin, P. M. Coelho, K. Lasek, F. A. Nugera, H. R. Gutiérrez, M. Batzill, *Chem. Mater.* **2021**, *33*, 8018.
[44] J. Li, S. Kolekar, M. Ghorbani-Asl, T. Lehnert, J. Biskupek, U. Kaiser, A. V. Krasheninnikov, M. Batzill, *ACS Nano* **2021**, *15*, 13249.
[45] L. Zhang, T. Yang, M. F. Sahdan, Arramel, W. Xu, K. Xing, Y. P. Feng, W. Zhang, Z. Wang, A. T. S. Wee, *Adv. Electron. Mater.* **2021**, *7*, 2100559.
[46] R. Gatensby, N. McEvoy, K. Lee, T. Hallam, N. C. Berner, E. Rezvani, S. Winters, M. O'Brien, G. S. Duesberg, *Appl. Surf. Sci.* **2014**, *297*, 139.

 © 2024 The Author(s). Advanced Electronic Materials published by Wiley-VCH GmbH

2199160x, 0, Downloaded from https://onlinelibrary.wiley.com/doi/10.1002/aelm.202400392 by Universitat der Bundeswehr Munchen, Wiley Online Library on [24/01/2025]. See the Terms and Conditions (https://onlinelibrary.wiley.com/terms-and-conditions) on Wiley Online Library for rules of use; OA articles are governed by the applicable Creative Commons License